

# Riemann solution for a class of morphodynamic shallow water dam-break problems

Fangfang Zhu<sup>1</sup>, Nicholas Dodd<sup>2</sup> †

<sup>1</sup>Department of Civil Engineering, Research Centre for Fluids and Thermal Engineering,  
University of Nottingham Ningbo China, Ningbo, 315100, China

<sup>2</sup>Faculty of Engineering, University of Nottingham, Nottingham NG7 2RD, UK

(Received ?; revised ?; accepted ?. - To be entered by editorial office)

This paper investigates a family of dam-break problems over an erodible bed. The hydrodynamics are described by the shallow water equations, and the bed change by a sediment conservation equation, coupled to the hydrodynamics by a sediment transport (bed load) law. When the initial states  $\bar{U}_l$  and  $\bar{U}_r$  are sufficiently close to each other the resulting solutions are consistent with the theory proposed by Lax (1973), that for a Riemann problem of  $n$  equations there are  $n$  waves associated with the  $n$  characteristic families. However, for wet-dry dam-break problems over a mobile bed, there are 3 governing equations, but only 2 waves. One wave vanishes because of the presence of the dry bed. When initial left and right bed levels ( $B_l$  and  $B_r$ ) are far apart, it is shown that a semi-characteristic shock may occur, which happens because, unlike in shallow water flow on a fixed bed, the flux function is non-convex. In these circumstances it is shown that it is necessary to reconsider the usual shock conditions. Instead, we propose an implied internal shock structure the concept of which originates from the fact that the stationary shock over fixed bed discontinuity can be regarded as a limiting case of flow over a sloping fixed bed. The Needham & Hey (1991) approximation for the ambiguous integral term  $\int h dB$  in the shock condition is improved based on this internal shock structure, such that mathematically valid solutions that incorporate a morphodynamic semi-characteristic shock are arrived at.

**Key words:** Authors should not enter keywords on the manuscript, as these must be chosen by the author during the online submission process and will then be added during the typesetting process (see <http://journals.cambridge.org/data/relatedlink/jfm-keywords.pdf> for the full list)

---

## 1. Introduction

A Riemann problem consists of an initial value problem composed of a set of conservation equations together with initial piecewise constant data having a single discontinuity.

In nonlinear shallow water flows, piecewise continuous solutions frequently develop. This is because the equations commonly used for describing them admit shocks (discontinuities) as solutions. These are usually interpreted as breaking waves (or bores), and therefore possess a straightforward physical significance, as well as a mathematical structure. These shocks are weak solutions in the sense that they satisfy the integral form

† Email address for correspondence: Nicholas.Dodd@nottingham.ac.uk.

39 of the flow equations. Smooth (differentiable) flow regions may be matched across these  
 40 shocks by shock conditions, which can be derived by considering mass and momentum  
 41 conservation across the shock.

42 Therefore, Riemann problems commonly occur in shallow water flows. Indeed, if one  
 43 interprets all data in a shallow water numerical model as being piecewise continuous,  
 44 then a whole series of such problems is solved at each time, and this interpretation forms  
 45 the basis of a class of numerical shallow water solvers (Toro 2001).

46 From a physical standpoint, Riemann solutions in shallow water flows are important  
 47 because they provide us with solutions to idealised problems that can be used as verifica-  
 48 tion cases for numerical solvers. Additionally, these idealised problems serve to highlight  
 49 fundamental shallow water dynamics. In shallow water flows a variety of Riemann prob-  
 50 lems are of interest. One of the simplest of these are dam-break problems, which comprise  
 51 a Riemann problem with zero initial velocities.

52 The simplest dam-break problem involves one wet and one dry side (wet-dry), and  
 53 with the point of discontinuity corresponding to the position of a notional dam wall that  
 54 at the initial time is instantaneously removed. Solution to this simplest shallow water  
 55 dam-break problem is given in Stoker (1957). Although one could insist that a dam-break  
 56 problem only be wet-dry, here we relax this description so as to include so-called wet-wet  
 57 dam-break problems. These more generalised dam-break problems have a richer structure  
 58 (see Toro 2001). We further consider dam-break problems in which the initial bed levels  
 59 also are different (see Bernetti *et al.* 2008).

60 The Riemann problems in Stoker (1957); Toro (2001); Bernetti *et al.* (2008) are those  
 61 with a fixed bed. If we allow the bed to become erodible, coupling flow velocity to move-  
 62 ment of sediment via a bed-load sediment transport relation, then a more complex picture  
 63 emerges. The solution of the shallow water mobile bed wet-dry dam-break problem with  
 64 no bed discontinuity at the dam location dates back to Fraccarollo & Capart (2002), who  
 65 considered a system with separate layers for fluid and sediment. The equivalent problem  
 66 without separate layers was considered by Kelly & Dodd (2009), amongst others. These  
 67 problems are also important from a physical perspective because in real dam-break events  
 68 considerable scour may result due to the high flow velocities.

69 In this paper we go further and consider generalised mobile-bed dam-break problems,  
 70 in which initial bed levels are not, in general, equal across the initial data: see figure  
 71 1. Aside from being important in the context of true dam-break events, they also have  
 72 relevance in the dynamics of waves on a beach. This is because a so-called backwash bore  
 73 (i.e., a hydraulic jump) is frequently created when water runs back down the beach after  
 74 a single wave uprush (Hibberd & Peregrine 1979). As the water drains the conditions at  
 75 the hydraulic jump may be such that flow is minimal and thus subsequent development  
 76 is predictable as a solution to a mobile-bed dam-break problem (Zhu & Dodd 2015).

77 Furthermore, we reconsider the usual shock conditions. For non-constant bed-levels  
 78 the bed-slope term in the flux-conservative form of the momentum equation is not in-  
 79 tegrable, necessitating approximation using conditions on each side of the shock. Here  
 80 we reinterpret this term based on a new approximation of the internal shock structure.  
 81 Although the motivation for this comes from the limiting case of flow over a sloping  
 82 bed (and against which we subsequently verify the method), we instead approximate the  
 83 internal morphodynamic shock structure as a series of sub-shock problems.

84 In the next section we present our governing equations, as well as some of the theory  
 85 governing the determination of the wave structure across the evolving Riemann solution.  
 86 We then use this theory to solve this class of Riemann problem in § 3. Finally we present  
 87 conclusions.

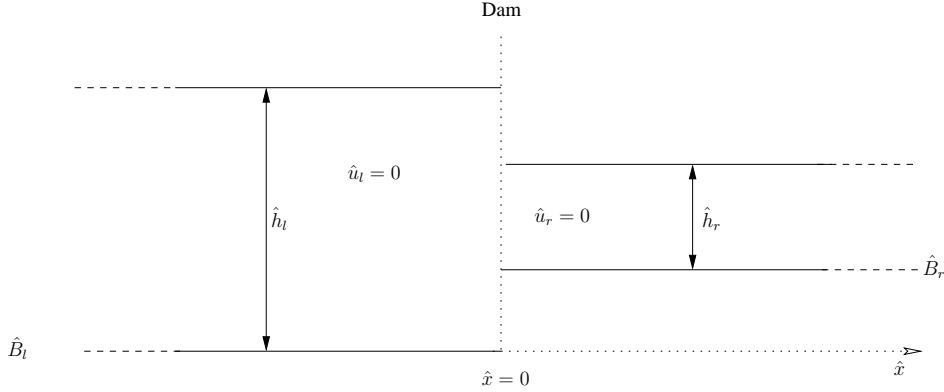


FIGURE 1. Schematic diagram for a dam-break problem.

## 2. Model development

### 2.1. Governing equations

A one dimensional (1D) idealised configuration for the initial set-up of a generalised dam-break problem is shown in figure 1. As mentioned, the nonlinear shallow water equations (NSWEs) have often been used for describing one- or two-dimensional dam-break flows (Ritter 1892; Stoker 1957; Toro 2001; Bernetti et al. 2008). For dam-break problems over a mobile bed, and if only bed load is considered (see Soulsby 1997), the governing equations are the NSWEs and a sediment conservation equation:

$$\hat{h}_{\hat{t}} + \hat{u}\hat{h}_{\hat{x}} + \hat{h}\hat{u}_{\hat{x}} = 0, \quad (2.1)$$

$$\hat{u}_{\hat{t}} + \hat{u}\hat{u}_{\hat{x}} + g\hat{h}_{\hat{x}} + g\hat{B}_{\hat{x}} = 0, \quad (2.2)$$

$$\hat{B}_{\hat{t}} + \xi\hat{q}_{\hat{x}} = 0, \quad (2.3)$$

where  $\hat{x}$  represents horizontal distance (m),  $\hat{t}$  is time (s),  $\hat{h}$  represents water depth (m),  $\hat{u}$  is a depth-averaged horizontal velocity ( $\text{ms}^{-1}$ ),  $\hat{B}$  is the bed level (m),  $\hat{q}$  is sediment flux due to bed load ( $\text{m}^2\text{s}^{-1}$ ),  $\xi = \frac{1}{1-p}$  with  $p$  being bed porosity, and  $g$  is acceleration due to gravity ( $\text{ms}^{-2}$ ).

In order to reveal the shock dynamics by solving a strictly hyperbolic system, we do not include the downslope diffusion effect in our model, although morphodynamic shocks are considered where vertical bed steps occur.

In general,  $\hat{q}$  is strongly dependent on  $\hat{u}$  and a weak function of  $\hat{h}$ . Here, a simple but commonly used formula  $\hat{q} = A\hat{u}^3$  (see Grass 1981) is employed for the bed load (see e.g. Kelly & Dodd 2010; Zhu et al. 2012), with  $A$  being the bed mobility parameter ( $\text{s}^2\text{m}^{-1}$ ). Note that this formulation is an over-simplification of the complex process of bed-load transport (see e.g. Pritchard & Hogg 2005) but that the purpose here is to construct the mathematical solution so that the basic dynamics can be understood, and to provide a mathematical test case for numerical models.

Therefore, (2.3) becomes

$$\hat{B}_{\hat{t}} + 3\xi A\hat{u}^2\hat{u}_{\hat{x}} = 0. \quad (2.4)$$

### 2.2. Non-dimensionalisation

The nondimensional variables are

$$x = \frac{\hat{x}}{\hat{h}_0}, t = \frac{\hat{t}}{\hat{h}_0^{1/2}g^{-1/2}}, h = \frac{\hat{h}}{\hat{h}_0}, u = \frac{\hat{u}}{\hat{u}_0} \text{ and } B = \frac{\hat{B}}{\hat{h}_0}, \quad (2.5)$$

113 where  $\hat{h}_0$  is a length scale, and  $\hat{u}_0 = (g\hat{h}_0)^{1/2}$ .

114 Substituting (2.5) into the governing equations (2.1), (2.2) and (2.4) gives

$$h_t + uh_x + hu_x = 0, \quad (2.6)$$

$$u_t + uu_x + h_x + B_x = 0, \quad (2.7)$$

$$B_t + 3\sigma u^2 u_x = 0, \quad (2.8)$$

115 where  $\sigma = \xi Ag$ .

116 The vector form of these three non-dimensional governing equations is

$$\vec{U}_t + \mathbf{A}(\vec{U})\vec{U}_x = 0 \quad (2.9)$$

117 with

$$\vec{U} = \begin{bmatrix} h \\ u \\ B \end{bmatrix}, \quad \mathbf{A}(\vec{U}) = \begin{bmatrix} u & h & 0 \\ 1 & u & 1 \\ 0 & 3\sigma u^2 & 0 \end{bmatrix}.$$

118 The eigenvalues of  $\mathbf{A}$  are the roots of the polynomial equation

$$\lambda^3 - 2u\lambda^2 + (u^2 - 3\sigma u^2 - h)\lambda + 3\sigma u^3 = 0. \quad (2.10)$$

119 Equation (2.10) has three roots, denoted  $\lambda_1$ ,  $\lambda_2$  and  $\lambda_3$  such that  $\lambda_1 \leq \lambda_3 \leq \lambda_2$ . For the  
120 solution of  $\lambda_1$ ,  $\lambda_2$  and  $\lambda_3$  we refer to Kelly & Dodd (2009, 2010).

### 121 2.3. Generalised simple wave theory

122 When there are two equations or fewer in a Riemann problem, we can derive a Riemann  
123 invariant along each characteristic (Stoker 1957). Jeffrey (1976) shows, however, that a  
124 direct extension of the concept of a Riemann invariant is not possible when there are  
125 more than two equations and dependent variables in a Riemann problem. Therefore, the  
126 generalised simple wave theory and the generalised Riemann invariants are introduced  
127 to solve such Riemann problems.

128 If we consider, for the moment, a general quasilinear hyperbolic system

$$\vec{U}_t + \mathbf{A}(\vec{U})\vec{U}_x = 0, \quad (2.11)$$

129 where  $\vec{U}$  is a vector of  $n$  dependent variables, given by

$$\vec{U} = [u_1, u_2, \dots, u_n]^T, \quad (2.12)$$

130 then the assumption that a simple wave region exists in a Riemann problem (or indeed  
131 generally) is such that  $\vec{U} = \vec{U}(u_1)$  holds across a wave, where  $u_1$  is chosen without loss  
132 of generality. This means that there is a functional dependence between  $u_i$  and  $u_1$  of the  
133 form  $u_i = f_i(u_1)$ , and the wave is called a generalised simple wave (Jeffrey 1976). For a  
134 simple wave, Eq. (2.11) can be written as,

$$\left( \frac{\partial u_1}{\partial t} \mathbf{I} + \frac{\partial u_1}{\partial x} \mathbf{A} \right) \frac{d\vec{U}}{du_1} = 0. \quad (2.13)$$

135 This system can have a non-trivial solution for  $d\vec{U}/du_1$  only if

$$|\mathbf{A} - \lambda_i \mathbf{I}| = 0, \quad (2.14)$$

136 where

$$\lambda_i = - \left( \frac{\partial u_1}{\partial t} \right) / \left( \frac{\partial u_1}{\partial x} \right), \quad i = 1, 2, \dots, n \Rightarrow \frac{du_1}{dt} = 0 \text{ along } \frac{dx}{dt} = \lambda_i. \quad (2.15)$$

137 This implies that  $u_1$ , and therefore  $u_i$ , are constant along characteristics  $\frac{dx}{dt} = \lambda_i$ , which  
 138 are themselves straight lines. A simple wave can also be defined as the wave, across which  
 139 one family of characteristics are all straight lines. There are  $n$  families of characteristics,  
 140 and the simple wave associated with the  $i^{\text{th}}$  characteristic family is called the  $\lambda_i$  simple  
 141 wave.

142 From Eq. (2.13), when  $\lambda = \lambda_i$  the vector  $\frac{d\vec{U}}{du_1}$  must be proportional to the right eigen-  
 143 vector  $\vec{R}^{(i)}$  of  $\mathbf{A}$ , which gives (Jeffrey 1976),

$$du_j = \frac{r_j^{(i)}}{r_1^{(i)}} du_1, j = 2, \dots, n, \quad (2.16)$$

144 where  $r_j^{(i)}$  is the  $j$ th component of  $\vec{R}^{(i)}$ .

145 Integrating (2.16) yields the  $j$ th generalised Riemann invariant  $K_j$  associated with the  
 146  $\lambda_i$  simple wave:

$$u_j - \int \frac{r_j^{(i)}}{r_1^{(i)}} du_1 = K_j, j = 2, \dots, n. \quad (2.17)$$

147 Further details of the simple wave theory can be found in Jeffrey (1976).

148 Returning to the present system we have:

$$\vec{R}^{(i)} = \begin{bmatrix} 1 \\ \frac{\lambda_i - u}{h} \\ \frac{(\lambda_i - u)^2}{h} - 1 \end{bmatrix}, \quad (2.18)$$

and

$$du = \frac{\lambda_i - u}{h} dh \quad (2.19)$$

$$dB = \left( \frac{(\lambda_i - u)^2}{h} - 1 \right) dh \quad (2.20)$$

149 For a fixed  $t$ , where  $h$  varies continuously, Eqs. (2.19) and (2.20) may be integrated  
 150 across the  $\lambda_i$  simple wave, in the  $(h, u, B)$  phase space, to yield the structure. However,  
 151 variables do not always vary continuously across the Riemann structure. Therefore, we  
 152 must understand the structure before we can solve it.

#### 2.4. Wave structure for a Riemann problem

153  
 154 In general the Riemann problem associated with Eq. (2.11), is composed of  $n$  waves  
 155 associated with the  $n$  characteristic families, which are separated by  $n - 1$  newly formed  
 156 constant regions provided that the values in the initial piecewise constant states are  
 157 sufficiently close (Toro 2009; Lax 1973; Fraccarollo & Capart 2002): see figure 2. Note  
 158 that a wave could be a rarefaction fan, a shock, or a contact wave.

159 As we integrate Eqs. (2.19) and (2.20) across a  $\lambda_i$  simple wave,  $\lambda_i$  varies such that  
 160  $d\lambda_i = \sum \frac{\partial \lambda_i}{\partial u_j} du_j$ , and in view of Eq. (2.16):

$$\frac{d\lambda_i}{du_1} = \vec{\nabla}_{\vec{U}} \lambda_i \cdot \vec{R}^{(i)} \quad (2.21)$$

161 where we have assumed, without loss of generality, that  $r_1^{(i)} = 1$ . Eq. (2.21) therefore  
 162 represents the rate of change of characteristic velocity across the  $\lambda_i$  wave. If

$$\vec{\nabla}_{\vec{U}} \lambda_i \cdot \vec{R}^{(i)} \neq 0 \text{ for all } \vec{U}, \quad (2.22)$$

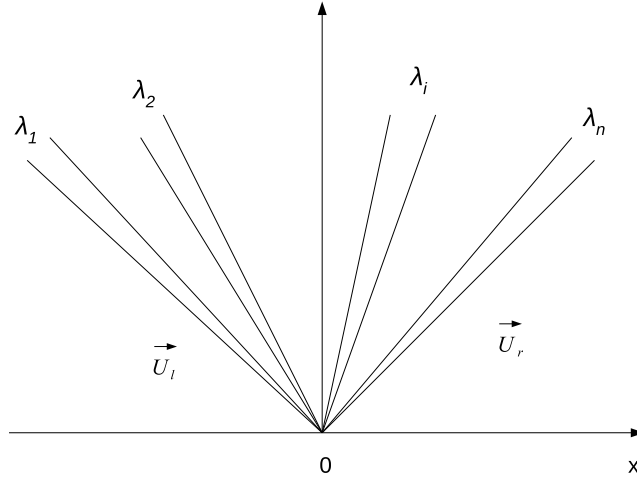


FIGURE 2. Wave structure for a Riemann problem with  $n$  characteristic families.

163 then the characteristic velocity increases or decreases continuously across the  $\lambda_i$  wave,  
 164 thus implying the existence of either an expansion (rarefaction) wave, or a compressive  
 165 wave (which becomes a shock ultimately). Then the  $\lambda_i$  wave field is said to be genuinely  
 166 nonlinear (or convex) (Sharma 2010). Note that if

$$\vec{\nabla}_{\vec{U}} \lambda_i \cdot \vec{R}^{(i)} = 0, \text{ for all } \vec{U}, \quad (2.23)$$

167 the wave field is said to be genuinely linear.

168 If we return again to the present system we find that

$$\vec{\nabla}_{\vec{U}} \lambda_i \cdot \vec{R}^{(i)} = \left\{ \lambda_i + \{2\lambda_i^2 - (2u - 6\sigma u) \lambda_i - 9\sigma u^2\} \frac{(u - \lambda_i)}{h} \right\} / G \quad (2.24)$$

169 where  $G = 3\lambda^2 - 4u\lambda + (u^2 - 3\sigma u^2 - h)$ , and it is therefore not clear that (2.24) will be  
 170 strictly  $>$  or  $<$  0. In this case the problem is said to be non-convex (Sharma 2010). Note  
 171 that this is in contrast to the classical (fixed bed) shallow water system, wherein

$$\vec{\nabla}_{\vec{U}} \lambda_{-,+} \cdot \vec{R}^{(-,+)} = \mp \frac{3}{2} \sqrt{\frac{1}{h}}. \quad (2.25)$$

172 This implies that the solution to the dam-break problem resulting from the system (2.6)–  
 173 (2.8) may possess semi-characteristic shocks (Sharma 2010).

### 174 2.5. Semi-characteristic shock

175 In general,  $\vec{\nabla}_{\vec{U}} \lambda_i \cdot \vec{R}^{(i)} = f(u_1)$  across a simple wave. If, as seems possible for Eq.  
 176 (2.24),  $f(u_1)$  passes through 0, this implies that at a rarefaction fan, across which char-  
 177 acteristics must diverge, a point is reached at which this can no longer happen because  
 178  $\frac{d\lambda_i}{du_1} = f(u_1) = 0$ . The only way then of accommodating this behaviour without the  
 179 solution becoming multivalued is for a shock to be contiguous with the fan: the semi-  
 180 characteristic shock, with the characteristic at one edge of the fan coinciding with this  
 181 semi-characteristic shock. The possible three wave structures are shown in figure 3. Note  
 182 that only (a) represents a physical structure in general. This is because for figure 3(b) and  
 183 (c) the structures will, in general, be overdetermined. For further details and exceptions  
 184 see Sharma (2010).

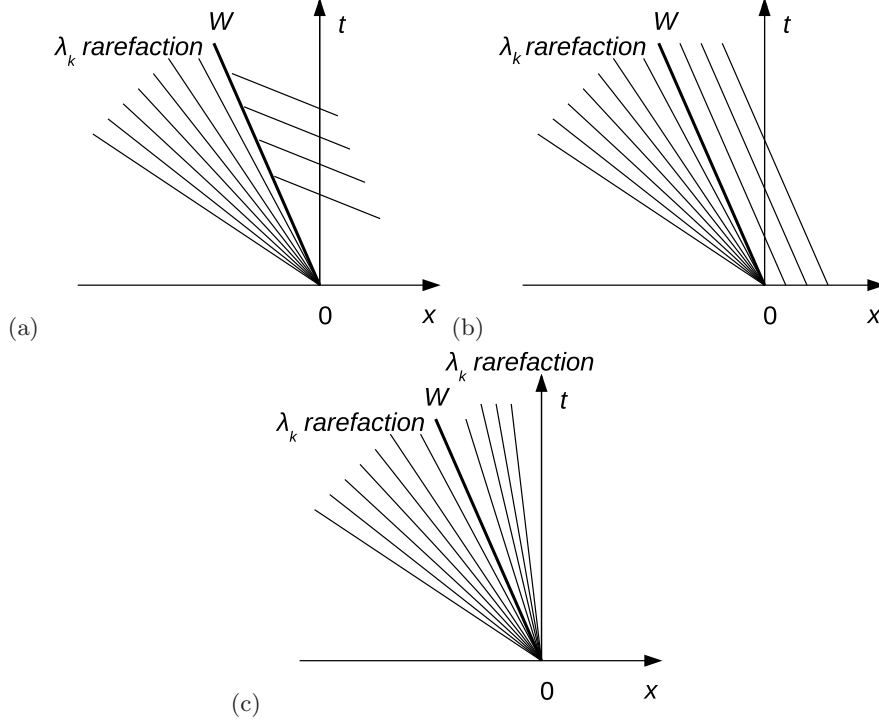


FIGURE 3. Schematic diagrams depicting possible structures for the combination of a rarefaction wave and a semi-characteristic shock within a simple wave.

185

### 2.6. Shock conditions

186 We require shock conditions to be satisfied across shocks and semi-characteristic shocks.  
 187 For derivations of the shock conditions we refer to Kelly & Dodd (2010); Zhu et al. (2012);  
 188 the shock conditions are

$$h_R u_R - h_L u_L - (h_R - h_L)W = 0, \quad (2.26)$$

$$W(h_R u_R - h_L u_L) - \left( h_R u_R^2 + \frac{h_R^2}{2} - h_L u_L^2 - \frac{h_L^2}{2} \right) - \int_{x_L}^{x_R} h B_x dx = 0, \quad (2.27)$$

$$(B_R - B_L)W - \sigma(u_R^3 - u_L^3) = 0, \quad (2.28)$$

189 where  $L$  and  $R$  represent variables on the left and right side of a shock, and  $W$  is shock  
 190 velocity.

191 The term  $\int_{x_L}^{x_R} h B_x dx = \int_{B_L}^{B_R} h dB$  is not uniquely determined, because  $h(x, t)$  is not  
 192 well defined along the face of bed step (Kelly 2009). Needham & Hey (1991) performed  
 193 the integration by approximation:

$$\int_{B_L}^{B_R} h dB \approx \frac{1}{2}(B_R - B_L)(h_R + h_L). \quad (2.29)$$

194 This expression is adopted by Kelly & Dodd (2010); Zhu et al. (2012); Zhu & Dodd  
 195 (2013, 2015).

196 Bernetti et al. (2008) equated it to the hydrostatic pressure force exerted on the bed

197 step by the water:

$$\int_{B_L}^{B_R} h dB = \begin{cases} \frac{1}{2}h_L^2 & \text{if } B_L + h_L \leq B_R \\ \frac{1}{2}(B_R - B_L)(2h_L + B_L - B_R) & \text{if } B_R \geq B_L \text{ and } B_L + h_L > B_R \\ \frac{1}{2}(B_R - B_L)(2h_R + B_R - B_L) & \text{if } B_R < B_L \text{ and } B_R + h_R > B_L \\ \frac{1}{2}h_R^2 & \text{if } B_R + h_R \leq B_L \end{cases} \quad (2.30)$$

198 There are four cases depending on from which side the water is exerting force on the  
199 bed step, and whether the free surface on the side of lower bed level is above the top of  
200 the bed step. Note that when free surface elevations on both sides are equal, Eqs. (2.29)  
201 and (2.30) are identical.

202 Different interpretations are possible. This can be seen by assuming that in the vicinity  
203 of a sudden change in bed level (a bed step)  $B = B_L + (B_R - B_L)H(x - x_0)$ , where  $H(x)$   
204 is the Heaviside function, so that

$$B_x = (B_R - B_L)\delta(x - x_0) \quad (2.31)$$

205 where  $\delta(x - x_0)$  is the Dirac delta function, and  $x = x_0$  is the location of the bed step.  
206 Using (2.31)

$$\int_{x_L}^{x_R} h B_x dx = (B_R - B_L)h(x_0). \quad (2.32)$$

207 Therefore, the remaining ambiguity is in how to define  $h(x_0)$ . From this perspective the  
208 expression of Needham & Hey (1991) (hereinafter NH91) is a simple average depth across  
209 the discontinuity; similarly, the middle two of the expressions of Bernetti et al. (2008)  
210 also correspond to composite depths, although the first and last cannot obviously be  
211 interpreted in this way. More generally, there is an implied variation of depth across the  
212 shock, which, it turns out, is important for the shocks we consider here.

### 213 2.7. Investigation of $\int_{x_L}^{x_R} h B_x dx$

214 If we know the internal structure of a shock, i.e.,  $h = h(B)$  across the shock, we can  
215 calculate the ambiguous integral numerically or analytically straightforwardly:

$$\int_{B_L}^{B_R} h dB \approx \sum_{i=0}^{n-1} \bar{h}_i \Delta B_i = \sum_{i=0}^{n-1} \frac{1}{2} (h_i + h_{i+1}) (B_{i+1} - B_i), \quad (2.33)$$

216 where  $h_i = h(B_i)$ ,  $B_0 \equiv B_L$ ,  $B_n \equiv B_R$ , and here we take  $\Delta B_i = \frac{B_R - B_L}{n}$ . When  $n = 1$ ,  
217 it is Needham & Hey (1991) approximation, i.e., (2.29). We refer to this approach as the  
218  $n$ -step approach; it is based on an implied internal structure of a shock. To see how this  
219 internal structure might be arrived at from a physical standpoint we now consider flow  
220 over a fixed bed slope.

#### 221 2.7.1. Interpretation of a stationary shock across a fixed bed discontinuity

222 We consider a steady state flow across a fixed, linear slope (see figure 4), and therefore  
223 only the hydrodynamic behaviour. From shallow water theory, the flow over the slope  
224 is either entirely sub- or supercritical (see Appendix D). We return here to dimensional  
225 variables, and then use an alternative non-dimensionalisation.

226 From continuity we have

$$\hat{h}(x)\hat{u}(x) = \hat{h}_L\hat{u}_L = \hat{q}_0. \quad (2.34)$$



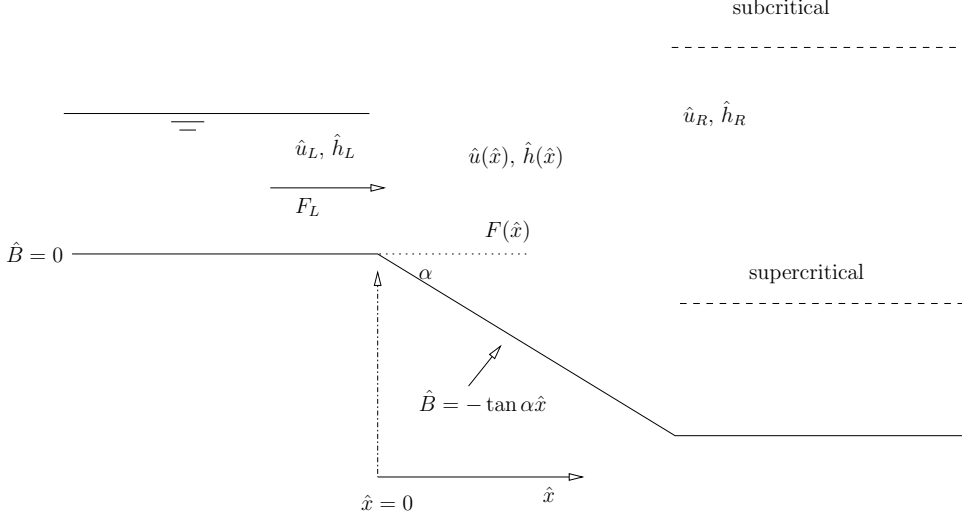


FIGURE 4. Bed level geometry for this case.  $F = \hat{u}/\sqrt{g\hat{h}}$  is the Froude number. In these scenarios the whole flow is either sub- or supercritical.

227 For a steady state, the flux-conservative form of (2.2) is

$$\left\{ \hat{h}\hat{u}^2 + \frac{1}{2}g\hat{h}^2 \right\}_{\hat{x}} = -g\hat{h}\hat{B}_{\hat{x}}. \quad (2.35)$$

228 Now we introduce a different set of nondimensional variables  $\tilde{h}$ ,  $\tilde{u}$ ,  $\tilde{x}$  and  $\tilde{B}$  on the sloping  
 229 section with  $\hat{h} = \hat{h}_L\tilde{h}$ ,  $\hat{u} = \hat{u}_L\tilde{u}$ ,  $\hat{x} = \hat{h}_L\tilde{x}/\tan\alpha$ , and  $\hat{B} = \hat{h}_L\tilde{B}$ . This gives:

$$\tilde{u} = \frac{1}{\tilde{h}}, \quad (2.36)$$

230

$$\tilde{B} = -\tilde{x}, \quad (2.37)$$

231 and

$$\left\{ F_L^2 \frac{1}{\tilde{h}} + \frac{1}{2}\tilde{h}^2 \right\}_{\tilde{x}} = -\tilde{h}\tilde{B}_{\tilde{x}} = \tilde{h}. \quad (2.38)$$

232 Note that the slope  $\tan\alpha$  is now absent, and the only free parameter is the inflow Froude  
 233 number,  $F_L$ .

234 Straightforwardly, we then obtain

$$\tilde{h} = 1 + \tilde{x} + \frac{1}{2}F_L^2 \frac{(\tilde{h}^2 - 1)}{\tilde{h}^2} = 1 - \tilde{B} + \frac{1}{2}F_L^2 \frac{(\tilde{h}^2 - 1)}{\tilde{h}^2} \quad (2.39)$$

235 for the variation of  $\tilde{h}$  across the slope. If we consider an abrupt change in bed level to  
 236 be the limiting case as  $\alpha \rightarrow \pi/2$  of this linear slope variation, and, moreover, that this  
 237 variation is independent of slope ( $\tan\alpha$ ), we may then assume that this variation may  
 238 be used across a fixed bed step as the implied internal shock structure.

239 It should be noted that (2.39) can also be directly derived from an energy conservation  
 240 law for the shallow water equations, because the flow down the slope is continuous. There  
 241 is some debate about whether energy conservation or the momentum balance equation,  
 242 in which  $\int_{\tilde{B}_L}^{\tilde{B}_R} \tilde{h}d\tilde{B}$  has to be approximated, should be used for the shock across a fixed  
 243 bed step (Valiani & Caleffi 2017; Cozzolino et al. 2011). The energy-conserving approach

244 has been widely used to study the stationary shock across a fixed bed discontinuity  
 245 (Karelskii & Petrosyan 2006; Valiani & Caleffi 2017). Valiani & Caleffi (2017) uses both  
 246 energy conservation and momentum balance to derive a depth at the bed step, i.e.,  $h(x_0)$   
 247 in (2.32). However, the energy loss across a morphodynamic shock is *a priori* unknown.  
 248 Therefore in this work, we utilise the momentum equation to solve the stationary shock  
 249 across a fixed bed step and also for morphodynamic shocks. Accordingly, we now focus  
 250 on the approximations for  $\int_{\tilde{B}_L}^{\tilde{B}_R} \tilde{h} d\tilde{B}$ .

251 (2.38) gives the exact solution of

$$\int_{\tilde{B}_L}^{\tilde{B}_R} \tilde{h} d\tilde{B} = - \left[ F_L^2 \frac{1}{\tilde{h}} + \frac{1}{2} \tilde{h}^2 \right]_L^R, \quad (2.40)$$

252 for a stationary shock across a fixed bed discontinuity, in which  $\tilde{h}$  is calculated using  
 253 (2.39).

254 The exact solution (2.40) together with (2.39) allows us to see how well (2.29), (2.30)  
 255 or (2.33) describe this usually ambiguous integral. The performances of these approxi-  
 256 mations are presented in Appendix A, from which we can see that (2.33) yields greater  
 257 accuracy than (2.29) or (2.30).

### 258 2.7.2. Application of $n$ -step approach to morphodynamic shocks

259 In this section we consider whether the  $n$ -step approach is valid for morphodynamic  
 260 shocks. Hereafter we return to the non-dimensionalisation introduced in § 2.2.

261 In the shallow water morphodynamical system that we consider here, there is in general  
 262 one characteristic speed much smaller than the other two. This can be seen in figure 5, in  
 263 which we plot  $\lambda' = \lambda/\sqrt{h}$  versus Froude number  $F = u/\sqrt{h}$ . Note that the characteristic  
 264 polynomial for  $\lambda'$  depends only on  $F$  and  $\sigma$ :

$$\lambda'^3 - 2F\lambda'^2 + ((1 - 3\sigma)F^2 - 1)\lambda' + 3\sigma F^3 = 0. \quad (2.41)$$

265 The characteristic speed that is generally much smaller than the other two is associated  
 266 with bed wave movement. This property pertains everywhere except for transcritical  
 267 flows, as also indicated in figure 5. Here we define a morphodynamic shock as a shock  
 268 formed by the convergence of two characteristics of one family, at least one of which is a  
 269 bed characteristic, and for which the shock speed  $|W| \ll 1$ .

270 Now, note that  $\sigma = \xi Ag \ll 1$  (see (2.8) and (2.28)). This is because  $\hat{q} = O(10^{-3})\text{m}^3/\text{s}/\text{m}$   
 271 or less, whereas  $\hat{u}_0 = O(1\text{m}/\text{s})$  in our original non-dimensionalisation (2.5). This implies  
 272 that at the hydrodynamical timescale  $\hat{t}_0 = \sqrt{\hat{h}_0/g}$ , (2.8) becomes  $B_t \approx 0$ , implying no  
 273 bed change at this timescale. However, at the morphodynamical timescale,  $\hat{t}_m = \hat{t}_0/\sigma$ ,  
 274  $\Rightarrow$  both sides of (2.28) are of comparable magnitude. This is consistent with  $W \ll 1$  for  
 275 a morphodynamic shock, so that in these circumstances (2.26)–(2.28) become

$$h_R u_R - h_L u_L \approx 0, \quad (2.42)$$

$$- \left( h_R u_R^2 + \frac{h_R^2}{2} - h_L u_L^2 - \frac{h_L^2}{2} \right) - \int_{x_L}^{x_R} h B_x dx \approx 0, \quad (2.43)$$

$$(B_R - B_L)W - \sigma(u_R^3 - u_L^3) = 0.$$

276 Note that (2.42) and (2.43) are the same shock conditions as those for flow over a fixed bed  
 277 step. This implies (2.39) can be derived from (2.42) and (2.43). This scaling is equivalent  
 278 to use of the quasi-steady approximation that is often used to study morphodynamics  
 279 (see e.g. Ribas et al. 2015). Therefore, we conclude that both (2.40) together with (2.39),  
 280 and (2.33) with (2.39) in § 2.7.1, which are both for a fixed bed stationary shock,

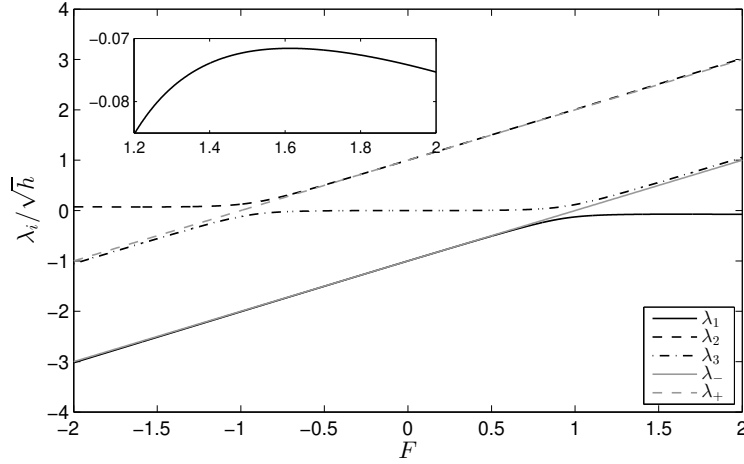


FIGURE 5. Dimensionless characteristic velocities for our system with  $\sigma = 0.01$  (after Zhu & Dodd (2015), figure 2).  $\lambda_{+,-}$  are the equivalent hydrodynamic (fixed bed) characteristic velocities.

281 can in principle be used as approximations for morphodynamic shocks with simplified  
 282 shock conditions (2.42), (2.43) and (2.28). Note that the conversion between different  
 283 non-dimensionalisations in §2.7.1 and § 2.2 should be done before applying (2.40) and  
 284 (2.39) for morphodynamic shocks.

285 By analogy, we can instead retain the  $W$  terms in (2.26) and (2.27) to obtain the  
 286 internal shock structures ( $h_i$ ,  $u_i$  and  $B_i$ ) and apply the  $n$ -step approach (2.33) for (2.26)–  
 287 (2.28). In the remainder of this paper we use this approach, which we refer to as the  
 288  $n$ -step approach, to construct the Riemann solution. The performances of these other  
 289 approximations for morphodynamic shocks are examined in Appendix C.

### 290 2.7.3. Implementation of $n$ -step approach for morphodynamic shocks

291 To use (2.33) across a morphodynamic shock with (2.26)–(2.28), the procedure is as  
 292 follows:

293 (a) Obtain initial estimates for  $\vec{U}_R = \vec{U}_R^{(1)}$  by solving (2.26)–(2.28), with  $\int_{x_L}^{x_R} hB_x dx$   
 294 approximated using (2.29).

295 (b)  $B_i$  values are then chosen according to  $B_L$  and  $B_R$ . Then  $h(B_i)$  and  $u(B_i)$  are  
 296 calculated according to (2.26) and (2.27) for the known  $B_i$ , by replacing  $(h, u, B)_{iL}$  and  
 297  $(h, u, B)_{iR}$  by  $(h, u, B)_{i-1}$  and  $(h, u, B)_i$ . Note that  $(h, u, B)_0 = (h, u, B)_L$ .

298 (c) Calculate the  $\int_{x_L}^{x_R} hB_x dx$  using the  $n$ -step approach (2.33).

299 (d) We then solve (2.26)–(2.28) using the calculated  $\int_{x_L}^{x_R} hB_x dx$  to get  $\vec{U}_R = \vec{U}_R^{(2)}$ .

300 (e) Repeat (b)–(d) until  $\vec{U}_R$  converges.

## 301 3. Solution of dam-break problems over an initially piecewise flat 302 mobile bed

303 The dam-break problem system consists of 3 equations, and according to Lax's theorem  
 304 (Lax 1973) there are at most 4 constant states separated by 3 elementary waves associated  
 305 with the 3 characteristic families. Note that for wet-dry dam-break problems over mobile  
 306 bed there are two waves separated by one newly formed constant region (Kelly & Dodd  
 307 2009). One wave vanishes because of the presence of the dry bed.

## 3.1. Initial conditions

The dimensional initial conditions for a generalised dam-break problem are shown in figure 1. With  $\hat{h}_0 = \hat{h}_l$ , the non-dimensional initial conditions of the left side are  $h(x \leq 0) = h_l = 1$ ,  $u(x \leq 0) = u_l = 0$ ,  $B(x \leq 0) = B_l = 0$ . For wet-dry dam-break problems,  $h(x \geq 0) = h_r = 0$ , and  $u(x \geq 0) = u_r = 0$ . For wet-wet dam-break problems, we set  $h(x \geq 0) = h_r = 0.1$ , and  $u(x \geq 0) = u_r = 0$ . In this paper, we consider conditions of both  $B_r = 0$  and  $B_r \neq 0$  to investigate the wave structures in these more generalised dam-break problems.

## 3.2. Wet-dry dam-break problem

We first assume that the wet-dry dam-break solution over an erodible bed for various  $B_r$  consists only of elementary waves, i.e., rarefaction waves or shocks. We introduce the semi-characteristic shock when the assumption no longer applies. The obtained wave structures at  $t = 1$  are shown in figure 6.

3.2.1.  $B_r \geq B_l$ 

Figure 6(a) and (b) show, respectively, water surface elevation and bed level, and velocity. The wave structure is that of a  $\lambda_1$  rarefaction wave, a constant region,  $\vec{U}_*$ , and a  $\lambda_3$  rarefaction wave, which is consistent with that presented by Kelly & Dodd (2009), who considered only  $B_r = B_l = 0$ . As  $B_r \rightarrow B_l + h_l$ ,  $B_* + h_* \rightarrow B_l + h_l$  and the extents of the  $\lambda_1$  and  $\lambda_3$  rarefaction waves decrease, and the solution (at  $t = 1$ ) resembles the initial conditions more. Note that the volume of water set in motion at time  $t$  is  $h_l |\lambda_1(h_l)| t$ , and is independent of  $B_r$  because the left edge of the  $\lambda_1$  fan ( $\lambda_1(h_l)$ ) is unaffected by changes in  $B_r$ . As the downstream elevation  $B_r$  increases, velocities across the Riemann solution decrease, as, therefore, does the sediment movement. As  $B_r$  increases, the flow in the constant region changes from supercritical (e.g., when  $B_r = 0$ ) to subcritical flow (e.g., when  $B_r = 0.4$  or  $0.8$ ), and the  $\lambda_3$  wave close to  $x = 0$  changes from a hydrodynamic into a bed wave.

In the  $\lambda_3$  rarefaction fan,

$$dB = \left( \frac{(\lambda_3 - u)^2}{h} - 1 \right) dh = - \frac{3\sigma u^2 (\lambda_3 - u)}{\lambda_3 h} dh \quad (3.1)$$

where (2.10) has been used. Thus, the large bed change that occurs near the dam location for  $B_r = 0.4$  or  $0.8$  is connected by the  $\lambda_3$  simple wave with  $\lambda_3 \rightarrow 0$  in (3.1). The lip of the initial bed discontinuity is eroded by the flow, and the initial discontinuity in bed level is transformed into a steep continuous variation. The small bed step (Kelly & Dodd 2010) at the flow tip ( $x = x_s(t)$ ) remains a feature of the solutions with decreasing height as flow velocity there decreases as  $B_r$  increases. For  $B_r = h_l + B_l$  no flow ensues, and there is no erosion.

The wave development is closely related to Froude number ( $F$ ), and Froude number acts as a proxy for position  $x$ . In figure 7(f), we show the relationship between  $F$  and  $x$ .  $F$  increases across the Riemann solution as  $x$  increases. In figure 7 (a) and (b) the three derived characteristic velocities  $\lambda' = \lambda/\sqrt{h}$  are plotted as a function of Froude number ( $F$ ). Again, note that the  $\lambda'$  curves are invariant for all dam-break solutions with  $\sigma = 0.01$  unless there is a discontinuity in  $F$  when a shock develops. In contrast, the black line superimposed on parts of these curves indicates the variation of  $\lambda'_1$  across the  $\lambda_1$  fan, and the variation of  $\lambda'_3$  across the  $\lambda_3$  fan, with the jump from one to the other also depicted, for  $B_r = 0$  and  $0.4$ . If we follow the (black)  $\lambda'_i$  values along the  $\lambda'_i$  curves in figure 7 (a) and (b) from  $F = 0$  we see that  $\lambda'_1$  increases as  $F$  increases for  $B_r = 0.4$  and  $0$ . For  $B_r = 0$  the jump from  $\lambda'_1$  to  $\lambda'_3$  for  $B_r \geq 0$ , which corresponds

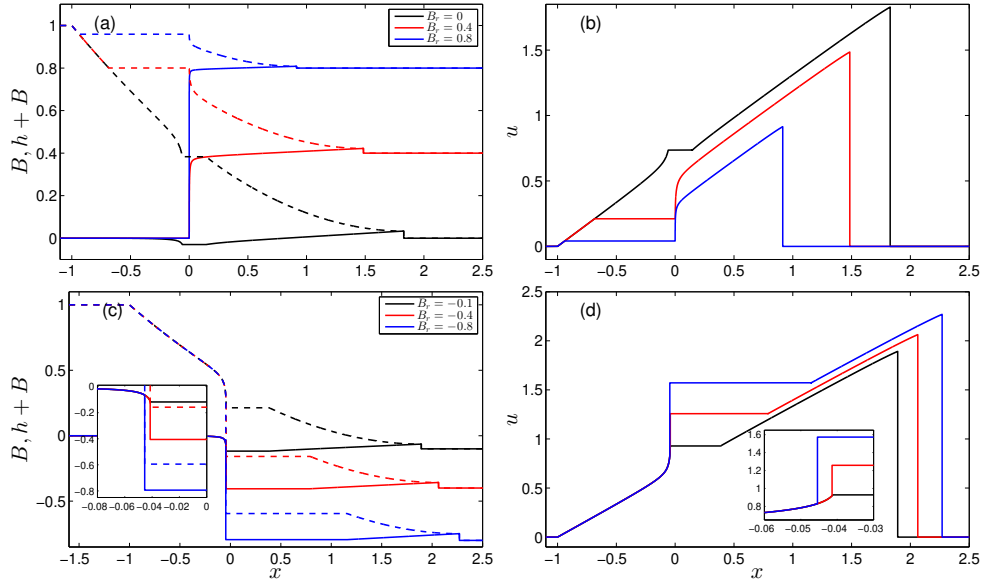


FIGURE 6. Structure of the wave solution for a wet-dry dam-break problem ( $h_l = 1$ ,  $u_l = 0$ ,  $B_l = 0$ ,  $h_r = 0$ ,  $u_r = 0$ , and  $\sigma = 0.01$ ) with varying  $B_r$  values ( $t = 1$ ). All semi-characteristic shocks are solved by the  $n$ -step approach for (2.26)–(2.28) with  $n = 2$ .

353 to the constant region, occurs for a larger  $F$  value than that for  $B_r = 0.4$ . Both jumps  
 354 occur prior to the point at which  $\frac{d\lambda'_1}{dF} = 0$ . Therefore,  $\lambda'$  increases monotonically across  
 355 both fans.  $\frac{d\lambda'_1}{dF} = 0$ , indicating a convergence in  $\lambda'_1$ , occurs at  $F \approx 1.6$  for all dam-break  
 356 solutions with  $\sigma = 0.01$ .

### 3.2.2. $B_r \leq B_l$

358 In figure 6(c) and (d) we can see the dam-break structure in this case, which is similar  
 359 to the preceding one in that two rarefaction fans ( $\lambda_1$  and  $\lambda_3$ ) form, separated by a  
 360 constant region.

361 Before commenting further on the structure of these solutions it is instructive first to  
 362 consider their representation in  $(\lambda', F)$  space. In figure 7(c)–(e) we do this. Figure 7(c)  
 363 and (d) illustrate the behaviour for  $B_r = -0.4$ . For figure 7(c) we see the elementary  
 364 wave solution. Note, however, that the jump via the constant region, from  $\lambda'_1$  to  $\lambda'_3$   
 365 curve, occurs when  $\frac{d\lambda'_1}{dF} < 0$ . This implies that at some point within the  $\lambda_1$  fan the  $\lambda'_1$   
 366 derived characteristics start decreasing as  $F$  increases. In contrast figure 7(d) shows the  
 367 behaviour with a semi-characteristic shock included.

368 Representing the solution in  $(\lambda', F)$  space is appealing because these curves are in-  
 369 variant with the continuous Riemann solution (i.e. size of bed step). However, it is the  
 370 convergence of  $\lambda_1$  characteristics (not  $\lambda'_1$ ) in the  $(x, t)$ -plane that determines whether  
 371 or not a semi-characteristic shock must be fitted. So, to determine this point of change  
 372 in the Riemann solution it is appropriate to examine variation in  $\lambda_1$ . The multivalued  
 373 solution of  $\lambda_1$  starts at  $B_r \approx -0.175$ , at the location at which  $F \approx 1.87$  (and  $h \approx 0.301$ ).  
 374 This point is illustrated in figure 8.  $\lambda_1$  increases as  $F$  increases, but at  $F \approx 1.87$  the  
 375 characteristic velocity ( $\lambda_1$ ) starts to decrease at the leading edge of the  $\lambda_1$  rarefaction  
 376 fan. The constant region, corresponding to the jump from  $\lambda_1$  to  $\lambda_3$  curve, thus occurs  
 377 when  $\frac{d\lambda_1}{dF} < 0$ . This indicates the convergence of  $\lambda_1$  characteristics within the  $\lambda_1$  fan.  
 378 The solution is multi-valued. The part of the  $\lambda_1$  curve for which  $F > 1$  behaves like a

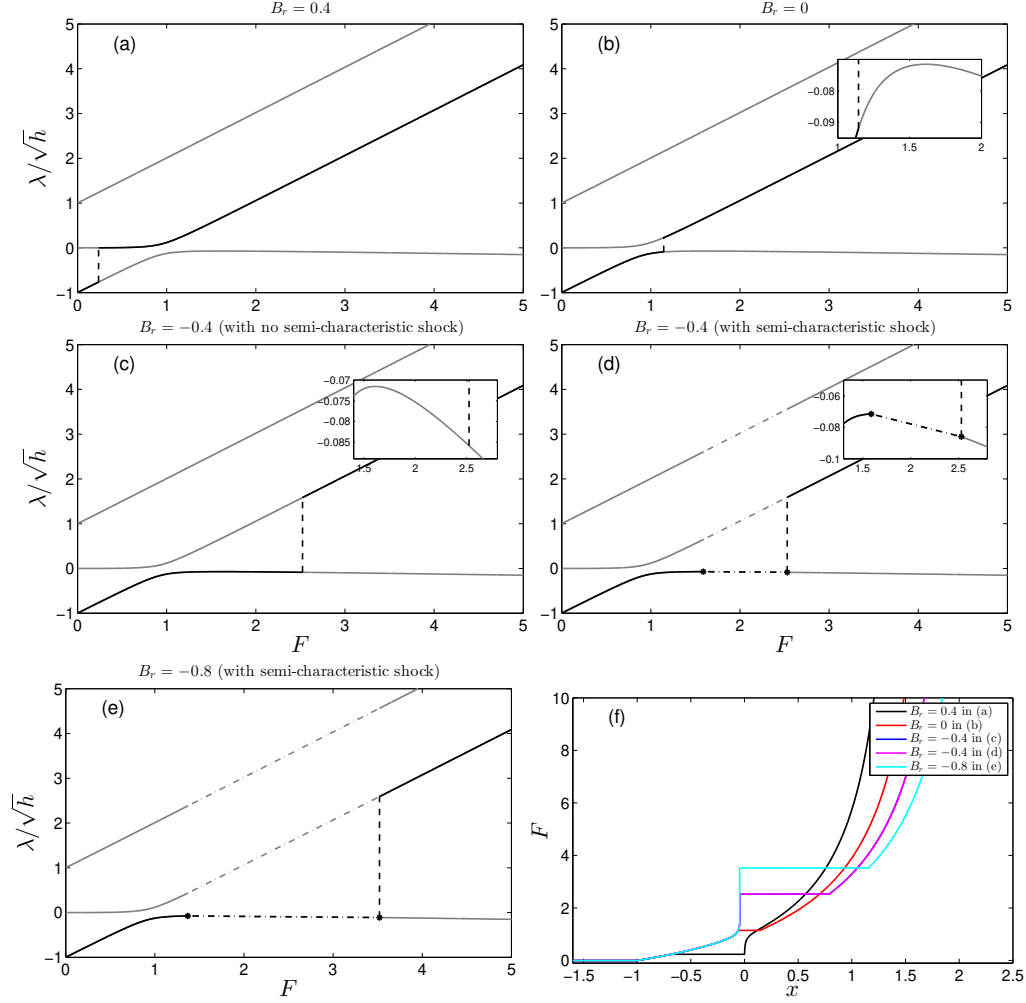


FIGURE 7. Illustrations of four of the Riemann solutions depicted in figure 6 in  $(\lambda/\sqrt{h}, F)$  space as the solution is traversed from  $x_l$  to  $x_s$ . Dashed lines represent the jumps from  $\lambda_1$  wave and  $\lambda_3$  wave. Dash-dotted lines represent the jump at the semi-characteristic shocks. (f) Illustration of how  $F$  varies across these solutions.

379 characteristic associated with a bed wave. Because  $\lambda_1 < 0$  this behaviour results in a bed  
 380 wave propagating against the flow. Similar behaviour can be observed in the propagation  
 381 of anti-dunes in supercritical open channel flow on a mobile bed, which propagate against  
 382 the flow (see Kennedy 1963).

383 To obtain a valid mathematical structure here, the  $\lambda_1$  fan must terminate prior to the  
 384 point at which  $\frac{d\lambda_1}{dh} = 0$  at a semi-characteristic shock with  $\lambda_{1L} = W$ ; downstream, in the  
 385 constant region we must have  $\lambda_{1R} < W$ , for a valid shock structure, which is possible  
 386 because  $F$  increases across the shock and therefore  $\lambda_1$  decreases.

387 Physically, the main difference between this case and that for  $B_r > B_l$  is the larger  
 388 velocities induced by the lower downstream elevation, which drives the early supercritical  
 389 flow development and therefore the formation of the semi-characteristic shock. Now, the  
 390 constant region is shifted mostly to  $x > 0$ , with a large decrease in  $h_*$ . The flow is  
 391 supercritical at the dam location, and the  $\lambda_1$  wave has become a bed wave close to

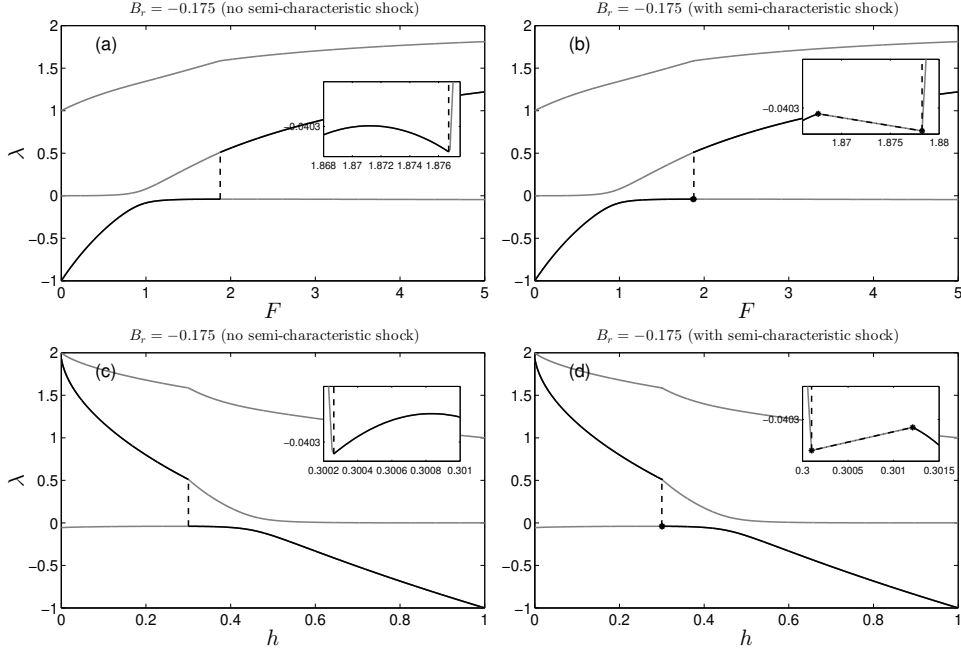


FIGURE 8. Illustrations of Riemann solutions for dam-break problem with  $h_l = 1$ ,  $u_l = 0$ ,  $B_l = 0$ ,  $h_r = 0$ ,  $u_r = 0$ ,  $B_r = 0.175$ , and  $\sigma = 0.01$  in  $(\lambda, F)$  and  $(\lambda, h)$  space to indicate why a semi-characteristic shock must be fitted. Dashed lines represent the jumps from  $\lambda_1$  wave and  $\lambda_3$  wave. Dash-dotted lines represent the jump at the semi-characteristic shocks. All semi-characteristic shocks are solved by the  $n$ -step approach for (2.26)–(2.28) with  $n = 2$ .

392  $x = 0$ , where we can also see the large bed change. The large bed decrease occurs at the  
 393 shock, which helps to connect widely separated values of  $B_l$  and  $B_r$ .

394 We assume an implied internal shock structure for all the semi-characteristic shocks,  
 395 and  $n = 2$  is adopted here. For the semi-characteristic shocks for all negative  $B_r$  values,  
 396 we have  $\lambda_{1L} = W > \lambda_{1R}$ . The convergence of characteristics implies that the shocks  
 397 are physical. Note that if we use the approximation (2.29) we do not arrive at physical  
 398 solutions for  $B_r = -0.8$ , and if we use the approximation (2.30) we do not get solutions  
 399 for any semi-characteristic shocks with the examined  $B_r$  values. It is therefore critical  
 400 that we introduce this more accurate approach. In Appendix C we show the equivalent  
 401 solutions and examine dependence on  $n$ .

### 402 3.2.3. Varying upstream bed level

403 We also examine the effect of varying the upstream bed level only, while keeping the  
 404 upstream surface elevation and downstream bed level fixed ( $h_l + B_l = 1$  and  $B_r = 0$ ).  
 405 The Riemann solutions ( $B$  and  $B + h$  only) are shown in figure 9. The structures are  
 406 similar to those already observed, but now with particularly large variations between  
 407 solutions for  $x < 0$ , because  $h_l$  varies and so therefore does the driving force.

408 The wave solutions of these dam-break problems are similar to those of fixed  $h_l$  and  
 409  $B_l$  values ( $h_l = 1$ ,  $B_l = 0$ ) but varying  $B_r$  values. Actually, these two kinds of dam-  
 410 break problems can be converted to each other through scaling and transformation. It  
 411 is the water depth on the left and bed difference that determines the wave structure.  
 412 Two dam-break problems with the same ratios of water depths and bed differences, i.e.,  
 413  $h_{l1}/h_{l2} = (B_{l1} - B_{r1})/(B_{l2} - B_{r2})$  are similar. Therefore the wave structures after dam  
 414 collapse are similar.

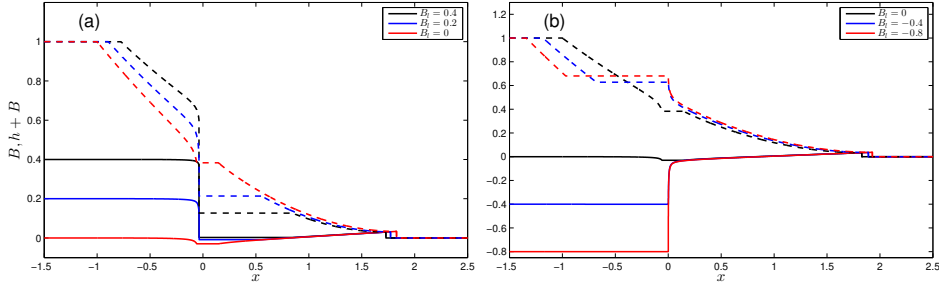


FIGURE 9. Solutions for dam-break problems with fixed upstream surface elevation ( $h_l + B_l = 1$ ) and downstream bed level ( $B_r = 0$ ) but varying  $B_l$  values. All semi-characteristic shocks are solved by the  $n$ -step approach for (2.26)–(2.28) with  $n = 2$ .

### 3.3. Wet-wet dam-break problem

415

416 We now turn to the wet-wet dam-break solution over an initially piecewise flat erodible  
 417 bed for various  $B_r$  values, which consists of elementary waves. The solutions at  $t = 1$  are  
 418 shown in figure 10.

#### 3.3.1. $B_r \geq B_l$

419

420 Figure 10(a) and (b) show, respectively, water surface level and bed level, and velocity  
 421 for this case. The wave structure is of a  $\lambda_1$  rarefaction wave, a  $\lambda_3$  rarefaction wave and  
 422 a  $\lambda_2$  shock. There are two newly formed constant regions ( $\vec{U}_{l*}$  and  $\vec{U}_{r*}$ ) separating the  
 423 three waves. For  $B_r = 0$ , the  $\lambda_2$  shock corresponds to the  $\lambda_+$  shock in the equivalent fixed  
 424 bed wet-wet dam-break problem (e.g. Toro 2001), and the  $\lambda_1$  and  $\lambda_3$  rarefaction waves  
 425 correspond to the  $\lambda_-$  rarefaction wave in the fixed bed case. When the bed mobility  
 426  $\sigma \rightarrow 0$ , the  $\lambda_1$  and  $\lambda_3$  rarefaction waves tend to combine into one wave.

427 As  $B_r$  increases, the  $\lambda_3$  wave becomes more confined to the original bed step position,  
 428 and less water flows into  $x > 0$  region. When  $h_r + B_r \rightarrow 1$  flow ceases.

#### 3.3.2. $B_r \leq B_l$

429

430 In figure 10(c) and (d), we can see the dam-break structure in this case. There is still  
 431 a  $\lambda_1$  rarefaction wave, and a  $\lambda_2$  shock, as for  $B_r > B_l$ . However, for the investigated  
 432 negative  $B_r$  values, the  $\lambda_3$  wave changes from a rarefaction wave into a shock. There are  
 433 also two newly formed constant regions. For  $B_r < 0$  as  $B_r$  decreases further (see figure  
 434 10(c)),  $h_{l*}$  decreases very quickly, and when  $h_{l*} < h_{r*}$  the  $\lambda_3$  fan observable for  $B_r = 0$   
 435 becomes a shock as the characteristics converge.

436 When  $B_r \lesssim -0.207$ , we get multivalued solutions within the  $\lambda_1$  fan, (see figure 10(c)).  
 437 The  $B_r$  value at which this occurs will depend on  $h_r$ , which here is 0.1, recall. We  
 438 again assume the existence of a  $\lambda_1$  semi-characteristic shock, and the corresponding wave  
 439 structure is shown in figure 10 (c) and (d). Once again, we assume an implied internal  
 440 shock structure, expressed through (2.33) in (2.26)–(2.28), in order to obtain a physical  
 441 shock (see Appendix C).

#### 3.3.3. Varying downstream water depth

442

443 In figure 11 we look at the effect that varying  $h_r$  has on the structure of these problems.  
 444 As  $h_r$  decreases, we expect this wet-wet problem to start to resemble previously examined  
 445 wet-dry problems (see figure 6). Accordingly, the  $\lambda_3$  shock diminishes such that between  
 446  $h_r = 0.03$  and 0.015 it becomes a rarefaction fan. As  $h_r$  decreases further the  $\lambda_3$  fan  
 447 extends towards the  $\lambda_2$  shock such that in the limit  $h_r \rightarrow 0$  the leading edge of this  $\lambda_3$



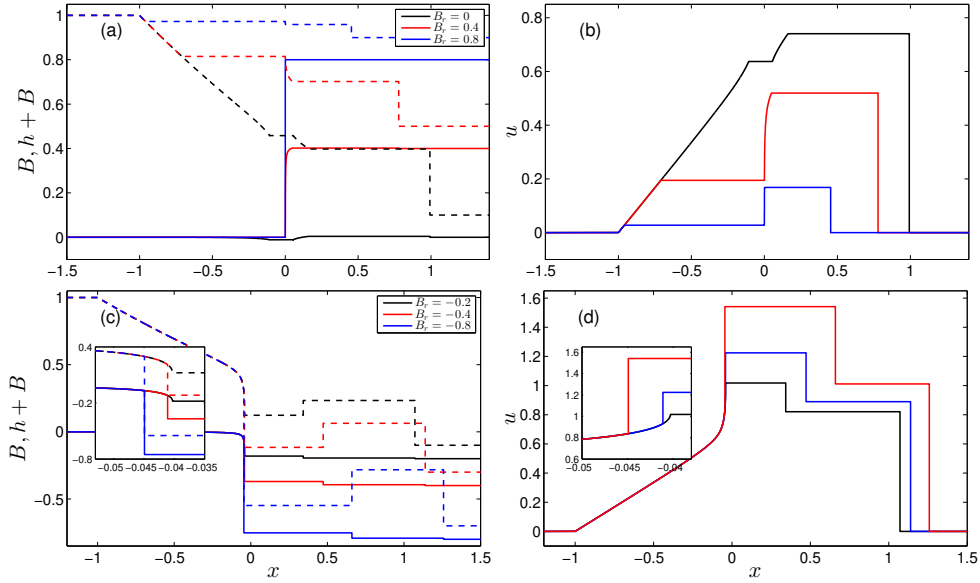


FIGURE 10. Structure of the wave solution for a wet-wet dam-break problem ( $h_l = 1$ ,  $u_l = 0$ ,  $B_l = 0$ ,  $h_r = 0.1$ ,  $u_r = 0$ , and  $\sigma = 0.01$ ) with varying  $B_r$  values at  $t = 1$ . All semi-characteristic shocks are solved by the  $n$ -step approach for (2.26)–(2.28) with  $n = 2$ .

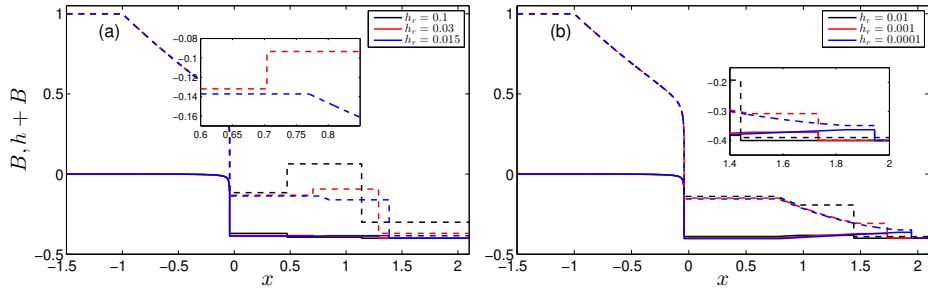


FIGURE 11. Structure of the wave solution for a wet-wet Riemann problem with ( $h_l = 1$ ,  $u_l = 0$ ,  $B_l = 0$ ,  $u_r = 0$ ,  $B_r = -0.4$  and  $\sigma = 0.01$ ) varying  $h_r$  values.

448 fan becomes the wet-dry boundary (with zero depth) and a semi-characteristic shock, and  
 449 the  $\lambda_2$  shock disappears. The  $\lambda_1$  wave is a combination of a fan and a semi-characteristic  
 450 shock, which is consistent with the equivalent wet-dry dam-break solution.

#### 451 4. Conclusion

452 Generalised wet-dry and wet-wet dam-break problems over an erodible, initially piece-  
 453 wise flat bed with water initially at rest and discontinuous bed levels are investigated and  
 454 solved based on the Riemann theory, and quasi-exact solutions are presented. The solu-  
 455 tions are consistent with the theory proposed by Lax (1973) that for a Riemann problem  
 456 of  $n$  equations there are at most  $n + 1$  constant states separated by  $n$  elementary waves  
 457 associated with the  $n$  characteristic families. However, for wet-dry dam-break problems,  
 458 one wave vanishes because of the presence of the dry bed. For the examined wet-dry  
 459 dam-break problems, there are 2 waves separated by 1 newly formed constant region,  
 460 which is in agreement with that in Kelly & Dodd (2009).

461 For some dam-break problems with negative bed steps, in which the initial states ( $B_l$   
462 and  $B_r$ ) are not sufficiently close, there are multivalued solutions when applying Lax's  
463 theorem. The semi-characteristic shock is introduced to describe the flow and physical  
464 wave structures are obtained. This is consistent with the solution for a Riemann problem  
465 of one single equation of non-convex flux function (Sharma 2010).

466 The ambiguous integral  $\int_{x_L}^{x_R} hB_x dx$  in shock conditions, which is usually approximated  
467 by the Needham & Hey (1991) approach, is reconsidered. An implied internal shock struc-  
468 ture is proposed initially by considering the limiting case of flow down a linear slope over  
469 fixed bed. Based on the internal shock structure, the integral  $\int_{x_L}^{x_R} hB_x dx$  is discretized  
470 into many steps and each step is approximated by Needham & Hey (1991) approach.  
471 This is to reduce the effects of curvature between  $h$  and  $B$ , which is source of inaccuracy  
472 in Needham & Hey (1991) approximation. This strategy is then extended to morphody-  
473 namic shocks which are here by assumption slow moving. However, because of the more  
474 general implied internal shock structure approach we ultimately adopt it would appear  
475 that this approach is more generally applicable. The resulting semi-characteristic shocks  
476 are physical, in that the characteristics converge across them.

477  
478 FZ and ND would like to acknowledge the financial support from both National Natural  
479 Science Foundation of China (Grant No. 51509135) and University of Nottingham Ningbo  
480 China (Small Research Grant). The authors would also like to thank the anonymous  
481 reviewers for their constructive comments.

## 482 Appendix A. Analysis of $\int_{\tilde{B}_L}^{\tilde{B}_R} \tilde{h} d\tilde{B}$ approximation methods

483 In this section, we analyse the performances of three approximation methods for the  
484 ambiguous term  $\int_{\tilde{B}_L}^{\tilde{B}_R} \tilde{h} d\tilde{B}$  (in the original nondimensional system  $\int_{B_L}^{B_R} h dB$  in shock con-  
485 dition (2.27)) on a linear (fixed) slope in §2.7: (2.29), (2.30) and (2.33) with (2.39) against  
486 the exact solution (2.40) with (2.39).

487 Here, we take  $\tilde{B}_L = 0$  and  $\tilde{B}_R = -\tilde{x}$ , with  $\tilde{x} > 0$  being a variable. The approximation  
488 (2.29) gives

$$\int_0^{-\tilde{x}} \tilde{h} d\tilde{B} = -\frac{1}{2}\tilde{x}(1 + \tilde{h}), \quad (\text{A } 1)$$

489 and it is exact if the relationship between  $\tilde{h}$  and  $\tilde{B}$  is linear. The approximation (2.30) is

$$\int_0^{-\tilde{x}} \tilde{h} d\tilde{B} = \begin{cases} -\frac{1}{2}\tilde{x}(2\tilde{h} - \tilde{x}) & \text{if } \tilde{B}_R < \tilde{B}_L \text{ and } \tilde{B}_R + \tilde{h}_R > \tilde{B}_L \\ -\frac{1}{2}\tilde{h}^2 & \text{if } \tilde{B}_R + \tilde{h}_R < \tilde{B}_L \end{cases} \quad (\text{A } 2)$$

490 We also use the  $n$ -step approach (2.33) with  $n = 5$  for the approximation

$$\int_0^{-\tilde{x}} \tilde{h} d\tilde{B} = -\frac{1}{2} \sum_{i=0}^{i=4} (\tilde{h}_i + \tilde{h}_{i+1}) (\tilde{B}_{i+1} - \tilde{B}_i) \quad (\text{A } 3)$$

491 with  $\tilde{B}_i = -i\tilde{x}/5$ , in which  $h_i$  is calculated by (2.39).

492 The results of (A 1), (A 2), (A 3) and (2.40) are illustrated in figure 12. Comparison  
493 shows that the approximation (A 1), i.e., (2.29), is generally quite accurate. Nearer to  
494 critical conditions the free surface curvature introduces significant discrepancies. Also, as  
495  $\tilde{B}_R - \tilde{B}_L$  increases, accuracy diminishes. The  $n$ -step approach (A 3), i.e., (2.33), greatly  
496 increased the accuracy. The approximation (A 2), i.e., (2.30) (Bernetti et al. 2008), is  
497 indistinguishable from the exact value when it is subcritical flow. It slightly overestimates

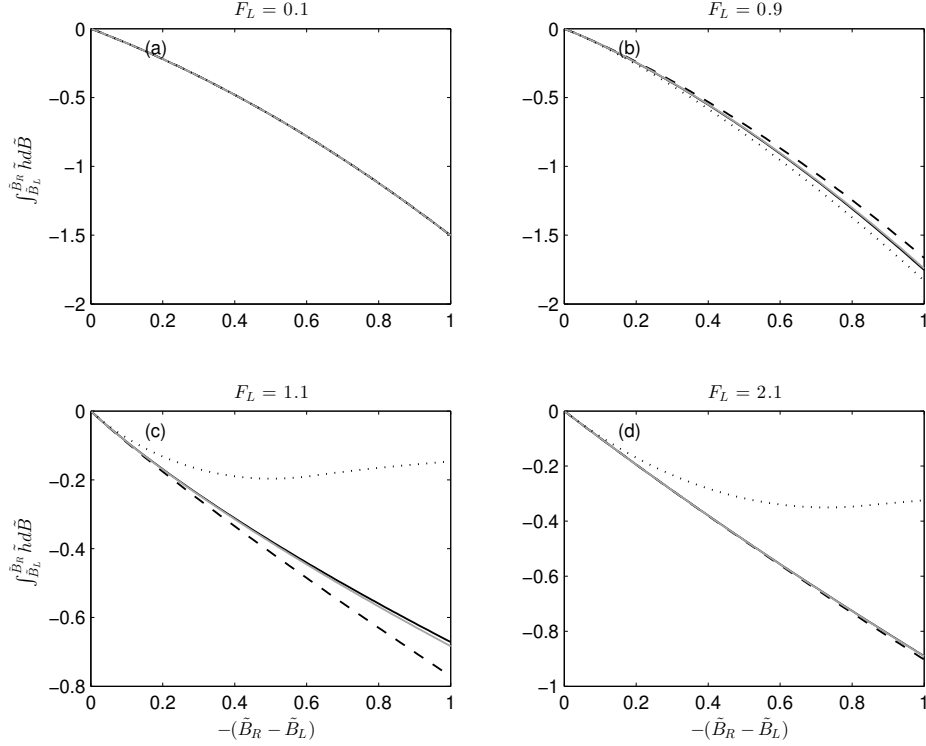


FIGURE 12.  $\int_{\tilde{B}_L}^{\tilde{B}_R} \tilde{h} d\tilde{B}$  plotted against size of bed step:  $\int_{\tilde{B}_L}^{\tilde{B}_R} \tilde{h} d\tilde{B} = - \left[ F_L^2 \frac{1}{h} + \frac{1}{2} \tilde{h}^2 \right]_L^R$  calculated using (2.39) (solid black line); that approximated by (A 1), i.e., (2.29) (dashed line), by (A 2), i.e., (2.30) (dotted line), and by (A 3), i.e., (2.33) with  $n = 5$  (grey solid line) for various Froude numbers.

498 the exact value when it is closer to critical flow. However, when the flow is supercritical,  
 499 the discrepancies become significant.

## 500 Appendix B. Comparison between wet-dry dam-break Riemann 501 solution of fixed and nearly fixed bed case

502 In this section, we test the Riemann solver by comparing the nearly fixed bed wet-dry  
 503 dam-break solution ( $\sigma = 1 \times 10^{-5}$ ) against the fixed bed solution.

504 The dam-break problem over a fixed bed with a bed step will lead to a stationary  
 505 shock at the bed step (Bernetti et al. 2008). For the positive  $B_r$  values examined, the  
 506 wave structure over a fixed bed from the left to right is a  $\lambda_-$  rarefaction wave, a constant  
 507 region, a stationary shock, and a  $\lambda_-$  rarefaction wave. That for the negative  $B_r$  values  
 508 examined, is a  $\lambda_-$  rarefaction wave, a stationary shock, a constant region, and a  $\lambda_-$   
 509 rarefaction wave (figure 13). This stationary shock corresponds to a semi-characteristic  
 510 shock if we interpret it in a morphodynamic context. It is a  $\lambda_3$  semi-characteristic shock  
 511 with  $\lambda_{3L} = W = \lambda_{3R} = 0$  because  $\sigma = 0$ .

512 On a nearly fixed bed, the wave structure for the non-negative  $B_r$  values examined, is  
 513 a  $\lambda_1$  rarefaction wave, a constant region and a  $\lambda_3$  rarefaction wave. The stationary shock  
 514 in the fixed bed case disappears because of the bed mobility, and the left part of the  $\lambda_3$

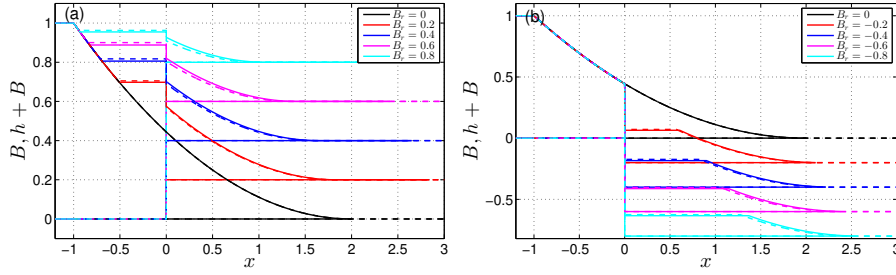


FIGURE 13. Comparison between wet-dry dam-break fixed bed ( $h_l = 1$ ,  $u_l = 0$ ,  $B_l = 0$ ,  $h_r = 0$ ,  $u_r = 0$ , and  $B_r = 0$ ) solution ( $\sigma = 0$ ; solid lines) and nearly fixed bed solution ( $\sigma = 1 \times 10^{-5}$ ; dashed lines). All semi-characteristic shocks are solved with NH91 approximation.

515 rarefaction wave becomes a steep but smooth part, which is to some extent similar to  
 516 the stationary shock in the fixed bed case. The nearly fixed bed solutions are in good  
 517 agreement with the fixed bed solutions (figure 13(a)).

518 The Riemann solutions with NH91 condition for the examined negative  $B_r$  values over  
 519 a nearly fixed bed are similar to those presented in § 3.2.2. The wave structures are a  $\lambda_1$   
 520 rarefaction, a  $\lambda_1$  semi-characteristic shock, and a  $\lambda_3$  rarefaction. The  $\lambda_1$  rarefaction fan  
 521 corresponds to the stationary shock on the fixed bed. The results compare favourably  
 522 with the corresponding fixed bed results (figure 13(b)).

### 523 Appendix C. Investigation of $\int_{B_L}^{B_R} h dB$ approximation methods in 524 dam-break problems

525 In this section, we investigate the approximation of  $\int_{B_L}^{B_R} h dB$  by comparing the solu-  
 526 tions of wet-dry and wet-wet dam-break problems using different approximation methods  
 527 (see Appendix A and §2.7.2). In summary, the approximation methods include (a): (2.40)  
 528 together with (2.39) and (2.28), i.e.,  $h_R$  and  $u_R$  are directly calculated for a known  $B_R$  as  
 529 for the stationary shock across fixed bed discontinuity; (b):  $n$ -step approach with (2.39)  
 530 applied in (2.42), (2.43) and (2.28) (c):  $n$ -step approach with (2.26)-(2.27) for  $h_i$ ,  $u_i$  and  
 531  $B_i$  for (2.26)-(2.28), (d): NH91 approximation (i.e.,  $n$ -step approach in method (c) with  
 532  $n = 1$ ; and (e): Bernetti et al. (2008) condition for (2.26)-(2.28) It should be noted that  
 533 with Bernetti et al. (2008) condition, we cannot find a solution if a semi-characteristic  
 534 shock is assumed, i.e., there is no alternative to the multi-valued solution.

535 The performances of the approximation methods for  $\int_{B_L}^{B_R} h dB$  are compared by exam-  
 536 ining wet-dry dam-break solutions for both  $B_r = -0.4$  and  $-0.8$ . In general, the approx-  
 537 imations give similar results for water levels and bed elevations when the whole solution  
 538 is shown. Differences can be seen at the semi-characteristic shock. When  $B_r = -0.4$ ,  
 539 method (a) and (b) give very similar results, and the results of method (c) and (d)  
 540 are close. When the bed step height increases, the difference grows. However, the semi-  
 541 characteristic shocks predicted by method (a) and (b) for  $B_r = -0.4$  (and  $B_r = -0.2$ ,  
 542 not shown) and that by method (d) for  $B_r = -0.8$  (and  $B_r = -0.6$ , not shown) are  
 543 non-physical because  $\lambda_{1L} \geq W \geq \lambda_{1R}$  cannot be satisfied. In contrast, method (c), used  
 544 throughout this paper, results in a physical semi-characteristic shock for all these  $B_r$ -  
 545 values. It is therefore necessary to retain the  $W$  terms in (2.26)-(2.28).

546 The effects of how many steps the integral  $\int_{B_L}^{B_R} h dB$  is discretized into are also investi-  
 547 gated. The comparison for both wet-dry and wet-wet dam-break problems using method  
 548 (c) ( $n$ -step approach) and (d) (NH91 approximation) is shown in figure 15. We can see

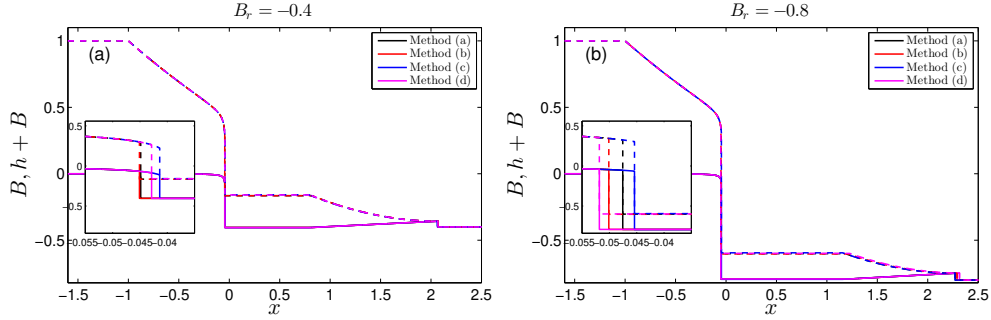


FIGURE 14. The comparison of wet-dry dam-break ( $h_L = 1$ ,  $u_L = 0$ ,  $B_L = 0$ ) solutions with different approximation methods for  $\int_{B_L}^{B_R} h dB$ . In the  $n$ -step approach in method (b) and (c),  $n = 2$ .

549 that the results with the implied internal shock structure are initially very close to those  
 550 directly using the NH91 approximation. As the size of bed step increases, the difference  
 551 between solutions with NH91 approximation and the new approach also increases slightly.

552 In the wet-dry dam-break problems with  $B_r = -0.2, -0.4$ , the semi-characteristic  
 553 shocks have  $\lambda_{1L} = W > \lambda_{1R}$  when solved directly with NH91 approximation. However,  
 554 as previously mentioned that for  $B_r = -0.6, -0.8$ , we have  $\lambda_{1L} = W < \lambda_{1R}$ , which  
 555 indicates a non-physical shock. It is further noted that in the  $B_r = -0.4, -0.6, -0.8$  cases,  
 556 the water on the left and right sides of the  $\lambda_1$  semi-characteristic shock are separated  
 557 by the high bed step (figure 16). Similarly, in the wet-wet dam-break problems with  
 558  $B_r = -0.6, -0.8$ , the semi-characteristic shocks are also non-physical. However, when we  
 559 use the implied internal shock structure, the shocks become physical.

560 In order to further investigate this, we take the wet-dry dam-break problem with  
 561  $B_r = -0.6$  as an example to illustrate the characteristics across the semi-characteristic  
 562 shocks; see figure 17. We can see the characteristics diverging when using the NH91 ap-  
 563 proximation, and characteristics converging when using implied internal shock structure.  
 564 This indicates that the NH91 approximation becomes less accurate when the bed step  
 565 becomes large in which the curvature of  $h$  with  $B$  becomes enhanced. In this case, the  
 566 importance of considering the internal shock structure becomes obvious.

567 In figure 18 we see how the multivalued problem in a wet-dry dam-break problem is  
 568 rationalised by introducing a semi-characteristic shock. According to Whitham (1974),  
 569 the areas  $\Delta A_1 = \Delta A_2$ . The results obtained here are consistent with this law, and when  
 570  $n$  increases,  $|\Delta A_1 - \Delta A_2|$  decreases. This also demonstrates that the  $n$ -step approach  
 571 applied for (2.26)-(2.28) gives more accuracy. Note that when the NH91 condition is used,  
 572 the jump at the semi-characteristic shock occurs outside the multi-valued region. As a  
 573 result, the shock becomes non-physical, because  $\lambda_{1*} > \lambda_{1L} = W$ .

#### 574 Appendix D. Impossibility of a smooth flow from sub- to 575 supercriticality down a slope

576 For smooth transition from sub- to supercriticality down a slope we need a situation  
 577 like that depicted in figure 19.

578 This flow is described by (2.38). Note that the RHS of (2.38)  $> 0$  for all  $\tilde{x}$ ; therefore  
 579 LHS  $> 0$  as well.

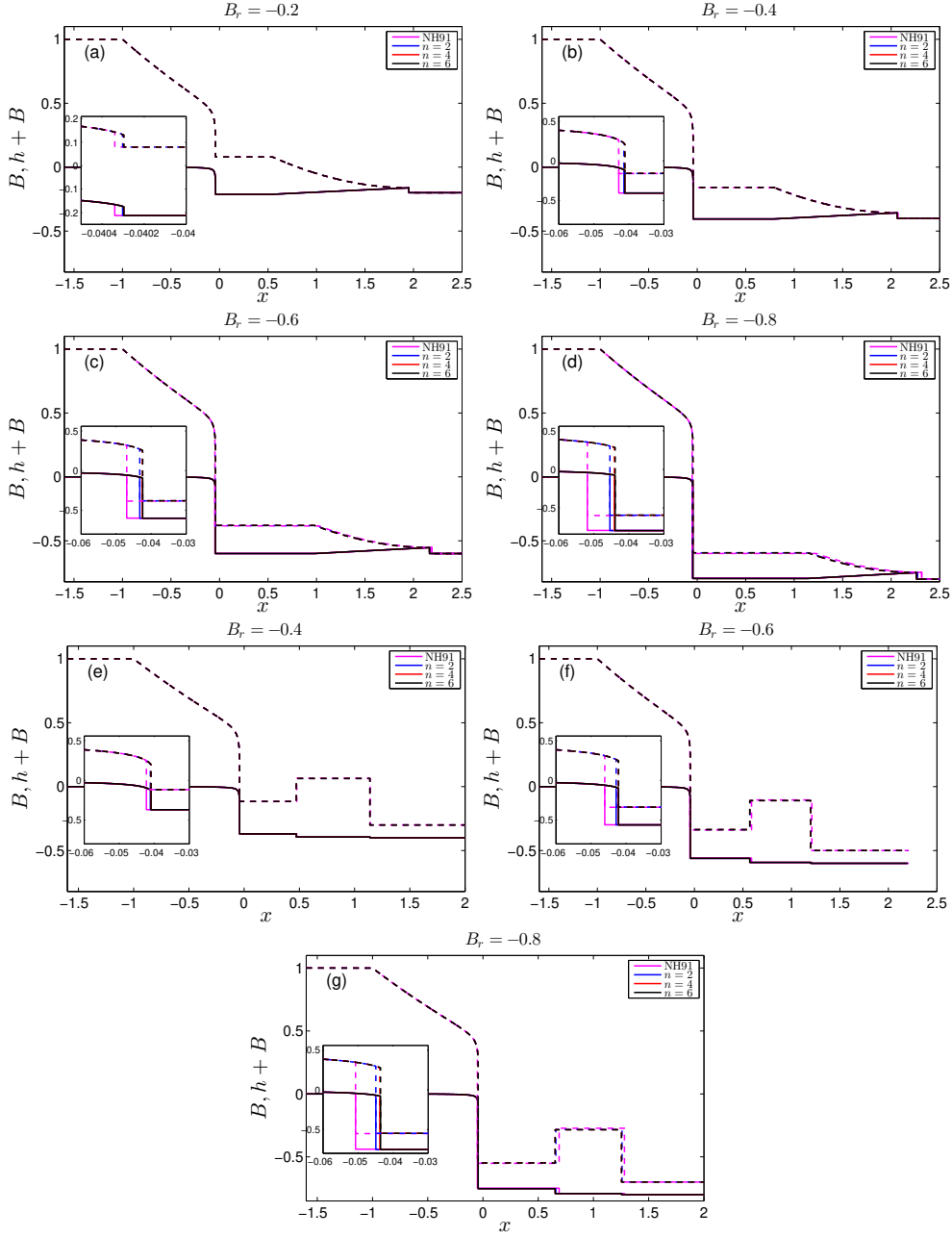


FIGURE 15. The comparison of dam-break solutions with NH91 approximation and those with the implied internal shock structure ( $n$ -step approach, for various  $n$  values). (a)–(d): wet-dry dam-break solutions; (e)–(g): wet-wet dam-break solutions.

If we differentiate the LHS of (2.38) w.r.t.  $x$  we get:

$$\begin{aligned}
 \tilde{h}\tilde{h}_{\tilde{x}} - F_L^2 \frac{\tilde{h}_{\tilde{x}}}{\tilde{h}^2} &= \tilde{h}_{\tilde{x}} \left\{ \tilde{h} - \frac{F_L^2}{\tilde{h}^2} \right\} \\
 &= \tilde{h}\tilde{h}_{\tilde{x}} \left\{ 1 - \frac{F_L^2}{\tilde{h}^3} \right\}
 \end{aligned} \tag{D1}$$

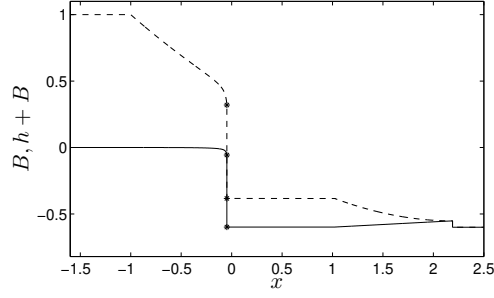


FIGURE 16. Structure of the wave solution (NH91 approximation) for a wet-dry dam-break problem with  $B_r = -0.6$  which shows that the water on the two sides of the semi-characteristic shock is separated by the high bed step ( $t = 1$ ).

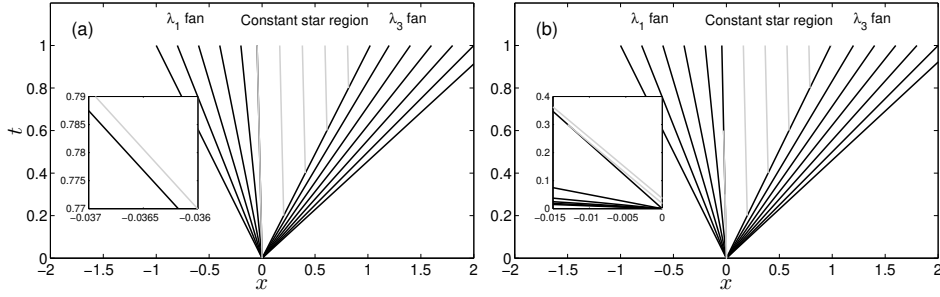


FIGURE 17. The characteristics set up for the dam-break solutions with  $B_r = -0.6$  with NH91 approximation (a) and  $n$ -step approach applied for (2.26)-(2.28) ( $n = 2$ ; b).

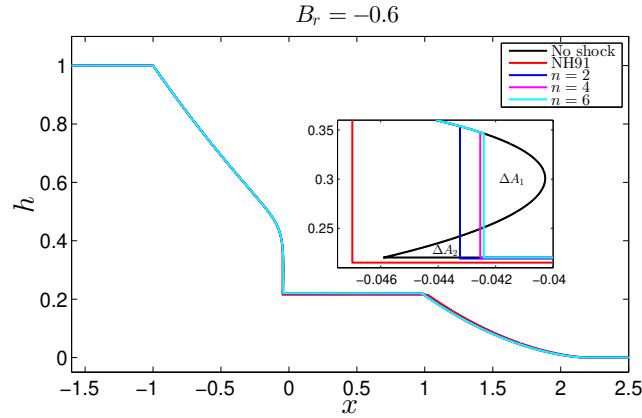


FIGURE 18. Multivalued profile and semi-characteristic shock fitting with NH91 approximation and  $n$ -step approach (2.33) for (2.26)-(2.28) in a wet-dry dam-break solution with  $B_r = -0.6$ .

However, for the flow in figure 19,  $\tilde{h}_{\tilde{x}} < 0$ . Therefore, we must have

$$1 - \frac{F_L^2}{\tilde{h}^3} < 0 \quad (\text{D } 2)$$

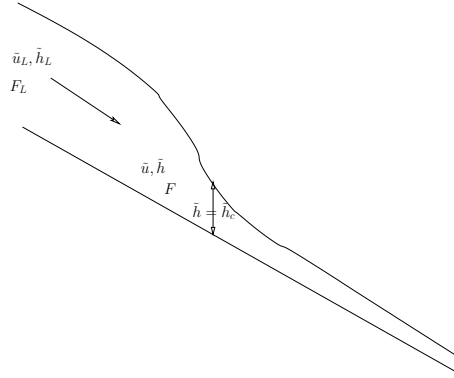


FIGURE 19. Smooth flow on a constant slope from sub- to supercritical conditions.

Now,

$$F^2 = \frac{\hat{u}^2}{g\hat{h}} = \frac{\hat{u}_L^2}{g\hat{h}_L} \frac{\tilde{u}^2}{\tilde{h}} = F_L^2 \frac{1}{\tilde{h}^3} \quad (\text{D } 3)$$

$$\Rightarrow \left\{ 1 - \frac{F_L^2}{\tilde{h}^3} \right\} = \{1 - F^2\} \quad (\text{D } 4)$$

580 Therefore, if flow is subcritical the flow cannot exist. Therefore, the flow in figure 19  
 581 cannot exist. The authors could not find an example in the literature of this analysis  
 582 being presented, hence its inclusion here.

#### REFERENCES

- 583 BERNETTI, R., TITAREV, V. A. & TORO, E. F. 2008 Exact solution of the riemann problem for  
 584 the shallow water equations with discontinuous bottom geometry. *J. Comput. Phys.* **227**,  
 585 3212–3243.
- 586 COZZOLINO, L., MORTE, R. D., COVELLI, C., GIUDICE, G. D. & PIANESE, D. 2011 Numerical  
 587 solution of the discontinuous-bottom shallow-water equations with hydrostatic pressure  
 588 distribution at the step. *Advances in Water Resources* **34**, 1413–1426.
- 589 FRACCAROLLO, L. & CAPART, H. 2002 Riemann wave descriptions of erosional dam break flows.  
 590 *J. Fluid Mech.* **461**, 183–228.
- 591 GRASS, A.J. 1981 Sediment transport by waves and currents. Technical Report FL29. University  
 592 College London, London Centre for Marine Technology.
- 593 HIBBERD, S. & PEREGRINE, D. H. 1979 Surf and run-up on a beach: A uniform bore. *J. Fluid*  
 594 *Mech.* **95**, 323–345.
- 595 JEFFREY, A. 1976 *Quasilinear hyperbolic systems and waves*. Pitman.
- 596 KARELSKII, K. V. & PETROSYAN, A. S. 2006 Problem of steady-state flow over a step in the  
 597 shallow-water approximation. *Fluid Dynamics* **41** (1), 12–20.
- 598 KELLY, D. M. 2009 Bore-driven swash on a mobile beach. PhD thesis, School of Civil Engineer-  
 599 ing, University of Nottingham, Nottingham, UK.
- 600 KELLY, D. M. & DODD, N. 2009 Floating grid characteristics method for unsteady flow over a  
 601 mobile bed. *Computers and Fluids* **38**, 899–909.
- 602 KELLY, D. M. & DODD, N. 2010 Beach face evolution in the swash zone. *J. Fluid Mech.* **661**,  
 603 316–340.
- 604 KENNEDY, J. F. 1963 The mechanics of dunes and antidunes in erodible-bed channels. *J. Fluid*  
 605 *Mech.* **16** (4), 521–544.
- 606 LAX, P. D. 1973 *Hyperbolic systems of conservation laws and the mathematical theory of shock*  
 607 *waves*. S.I.A.M.



- 608 NEEDHAM, D. J. & HEY, R. D. 1991 On nonlinear simple waves in alluvial river flows: a theory  
609 for sediment bores. *Phil. Trans. Roy. Soc. Lond. A* **334**, 25–53.
- 610 PRITCHARD, D. & HOGG, A. J. 2005 On the transport of suspended sediment by a swash event  
611 on a plane beach. *Coastal Eng.* **52**, 1–23.
- 612 RIBAS, F., FALQUÉS, A., DE SWART, H. E., DODD, N., GARNIER, R. & CALVETE, D. 2015 Un-  
613 derstanding coastal morphodynamic patterns from depth-averaged sediment concentration.  
614 *Rev. Geophys.* **53**, 362–410.
- 615 RITTER, A. 1892 Die fortpflanzung der wasserwellen. *Vereine Deutcher Ingenieure Zeitschrift*  
616 **36**, 947–954.
- 617 SHARMA, V. D. 2010 *Quasilinear Hyperbolic Systems, Compressible Flows, and Waves*. CRC  
618 Press.
- 619 SOULSBY, R. L. 1997 Dynamics of marine sands. a manual for practical applications. SR 466.  
620 Hydraulics Research Wallingford, Wallingford, England.
- 621 STOKER, J.J. 1957 *Water Waves*. New York, N.Y.: Interscience.
- 622 TORO, E. F. 2001 *Shock-capturing methods for free-surface shallow flows*. New York, NY.:  
623 Wiley.
- 624 TORO, E. F. 2009 *Riemann solvers and numerical methods for fluid dynamics*, 3rd edn. Berlin:  
625 Springer.
- 626 VALIANI, A. & CALEFFI, V. 2017 Momentum balance in the shallow water equations on bottom  
627 discontinuities. *Advances in Water Resources* **100**, 1–13.
- 628 WHITHAM, G. B. 1974 *Linear and Nonlinear Waves*. New York: Wiley-Interscience.
- 629 ZHU, F. & DODD, N. 2013 Net beach change in the swash: A numerical investigation. *Advances*  
630 *in Water Resources* **53**, 12–22.
- 631 ZHU, F. & DODD, N. 2015 The morphodynamics of a swash event on an erodible beach. *J.*  
632 *Fluid Mech.* **762**, 110–140.
- 633 ZHU, F., DODD, N. & BRIGANTI, R. 2012 Impact of a uniform bore on an erodible beach.  
634 *Coastal Eng.* **60**, 326–333.